

## Supporting information

### High-performance photodetector based on small-bundled single-wall carbon nanotube film/silicon heterojunctions

Yi-Ming Zhao<sup>a,b#</sup>, Xian-Gang Hu<sup>a,c#</sup>, Chao Shi<sup>a,b</sup>, Wu-Tong Ding<sup>a,b</sup>, Peng-Xiang Hou<sup>a,b\*</sup>,  
Chang Liu<sup>a,b\*</sup>, Hui-Ming Cheng<sup>a,d</sup>

<sup>a</sup> Shenyang National Laboratory for Materials Science, Institute of Metal Research, Chinese Academy of Sciences, Shenyang 110016, PR China.

<sup>b</sup> School of Materials Science and Engineering, University of Science and Technology of China, Shenyang, 110016, PR China.

<sup>c</sup> Advanced Interdisciplinary Research Center for Flexible Electronics, Academy of Advanced Interdisciplinary Research, Xidian University, Xi'an 710071, P. R. China

<sup>d</sup> Faculty of Materials Science and Engineering/Institute of Technology for Carbon Neutrality, Shenzhen Institute of Advanced Technology, Chinese Academy of Sciences, Shenzhen 518055, PR China.

#These authors were equal major contributors to this work.

\*Corresponding Authors: pxhou@imr.ac.cn (P.X. Hou) or cliu@imr.ac.cn (C. Liu).

## Experimental section

### *1. Synthesis of SWCNT films*

SB-SWCNT films with a carbon-welded structure were synthesized by using a FCCVD method at 1100 °C (Fig. S1), and the transparencies of the films were obtained by controlling the film collection time (Fig. S2). Ethylene (10-12 sccm) and hydrogen (5500-7000 sccm) were used as a carbon source and a carrier gas, respectively. A syringe pump was used to inject a mixture of liquid carbon source (toluene), catalyst precursor (ferrocene) and growth promoter (thiophene) with a weight ratio of 10: 0.3: 0.045 into a quartz tube reactor inserted into a vertical tubular furnace for SWCNT growth. A membrane filter was equipped at the downstream of the reactor to collect the SWCNT film. The thickness of the film was controlled by tuning the collection time.

### *2. Fabrication of photodetector device*

A n-type Si (100) wafer covered with a 300 nm-thick silicon oxide layer was first patterned with square windows. Then, the SiO<sub>2</sub> layer was etched away with a HF aqueous solution. We constructed a series of photodetectors with window areas of 9 mm<sup>2</sup>, 25 mm<sup>2</sup>, 100 mm<sup>2</sup> and 900 mm<sup>2</sup>. As-prepared SWCNT film was press-transferred onto the window, alcohol was dropped on the SWCNT film, and the membrane filter was removed. An insulating layer was then formed on the Si wafer by exposing to air at 60 °C for 12 h to form a thin layer of silica. Silver paste was painted around the active area to serve as the upper electrode, and a gallium–indium eutectic was used to form ohmic contact on the back of the silicon and to serve as the back electrode.

### *3. Characterization and Photoelectric measurements*

Laser Raman measurements were performed using a Jobin-Yvon Labram HR800 instrument with laser wavelengths of 532 nm and 633 nm. The microstructure of the SWCNT film was characterized by SEM (Nova Nano SEM 430) and TEM (JEM-2010HR and Tecnai G2 F20, operated at 200 kV). The surface roughness, morphology and surface potential of the samples were characterized using Atomic Force Microscopy (AFM, MultiMode 8). The thickness of the film with different transmittance was measured by surface profiler (KLA-Tencor P7). The

optical transmission spectra of a film were measured using a UV-Vis-NIR spectrophotometer (AGILENT CARY 5000). A Keysight B1500A semiconductor analysis tester was used to measure the photo response and current-voltage (I-V) characteristics of the photodetector. All tests were conducted at room temperature under normal pressure. The wavelengths of the lasers were adjustable in the range of 540~1090 nm. A light spot with a diameter of 2-3 mm was positioned at the active window center of the photodetector.

#### 4. Calculation process of the important parameter

**Responsivity (R):** A parameter that evaluates the ability of the photodetector to generate photocurrent or photovoltage. It is defined as the ratio of the photocurrent or photovoltage to the power of the incident laser ( $P_{in}$ ):

$$R = \frac{I_{ph} - I_d}{P_{in}} \text{ or } R = \frac{V_{ph} - V_d}{P_{in}} \quad (1)$$

where  $I_{ph}$  and  $I_d$  (or  $V_{ph}$  and  $V_d$ ) are the currents (or the voltages) under illumination and in the dark, respectively.

**Noise equivalent power (NEP):** NEP is one of the important indices to characterize the sensitivity of photodetectors. It is defined as the incident light power value when the signal-to-noise ratio of the device is equal to 1 in the 1 Hz output bandwidth:

$$NEP = \frac{\sqrt{(I_{noise})^2 / 1 \text{ Hz}}}{R} \quad (2)$$

where  $I_{noise}$  is noise current. It is equivalent to the dark current ( $I_d$ ) in this paper, and its units are  $\text{WHz}^{1/2}$ .

**Detectivity ( $D^*$ ):**  $D^*$  is widely used to compare the performance of the different photodetectors with different activities, geometries and working mechanisms, and represents the ability of photodetectors to detect weak light signals. The higher the  $D^*$  value, the better the detection performance of the photodetector. It is an important parameter, and the specific calculation method is:

$$D^* = \frac{\sqrt{A}}{NEP} \quad (3)$$

$D^*$  and NEP are reciprocals of each other. In order to facilitate the calculation,  $D^*$  can also

be calculated approximately as:

$$D^* = \frac{R\sqrt{A}}{\sqrt{2eI_d}} \quad (4)$$

Here,  $A$  is the active area of the photodetector (in this paper,  $A$  is about  $0.09 \text{ cm}^2$ ),  $e$  is elementary charge ( $1.6 \times 10^{-19} \text{ C}$ ), and the units of  $D^*$  are  $\text{cmHz}^{1/2}\text{W}^{-1}$ (Jones).

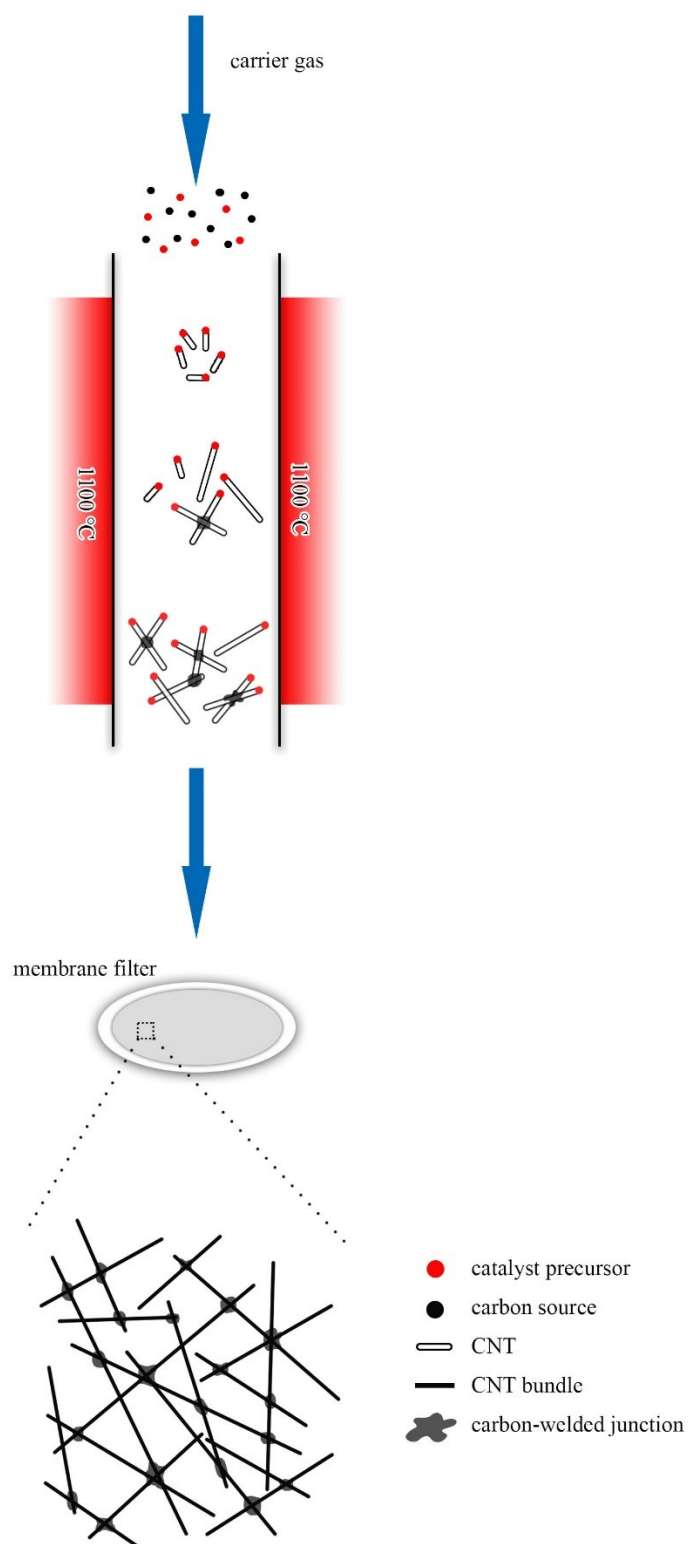


**Fig. S1.** Schematic of the experimental setup for the synthesis of SB-SWCNT films with carbon-welded junctions.

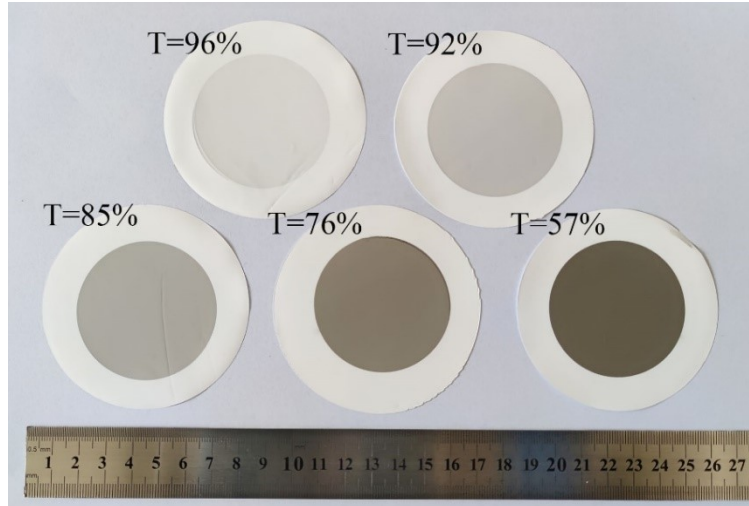


**Fig. S2.** Optical images of the SWCNT films with different transmittances (T).

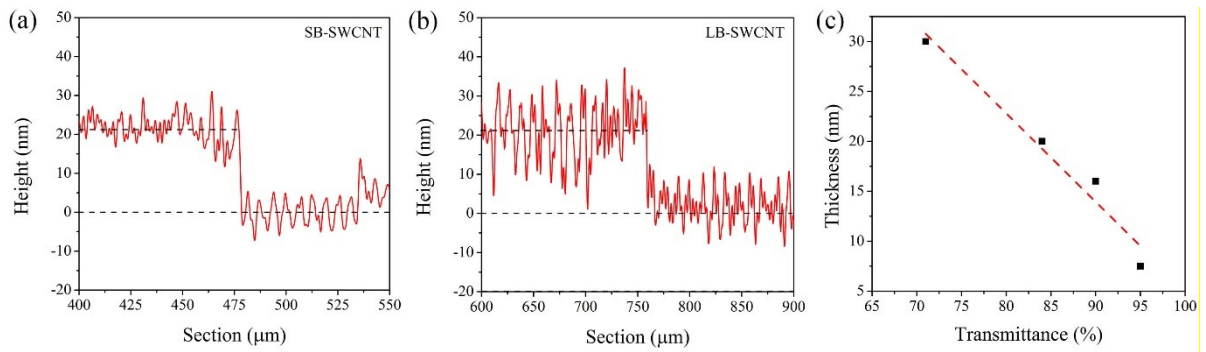


**Fig. S3.** (a) Dependence of transmittance on the thickness of the SB-SWCNT films. The thicknesses of the (b) SB-SWCNT films and (c) LB-SWCNT films with a transmittance of 84%.

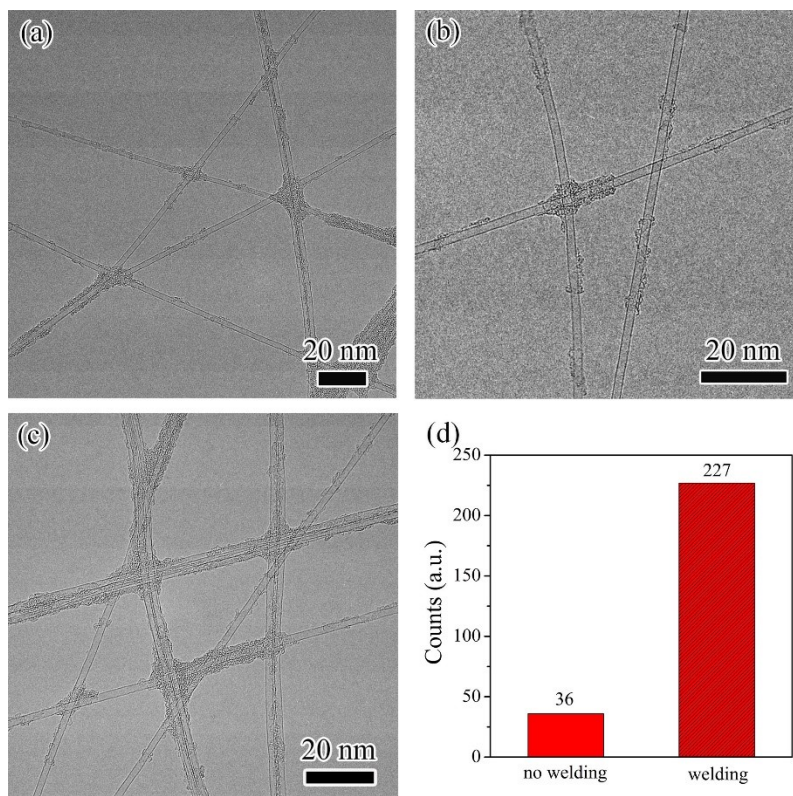


**Fig. S4.** (a-c) Typical TEM images of SB-SWCNTs and (d) a statistical number of junctions with and without carbon-welding in the network.

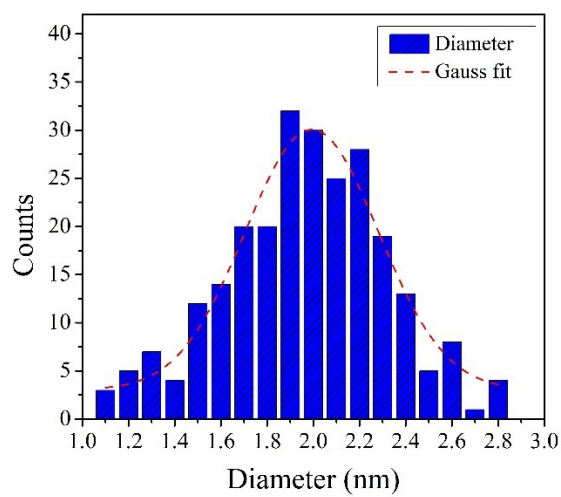


**Fig. S5.** Tube size distribution of the SB-SWCNTs as characterized by TEM observation.

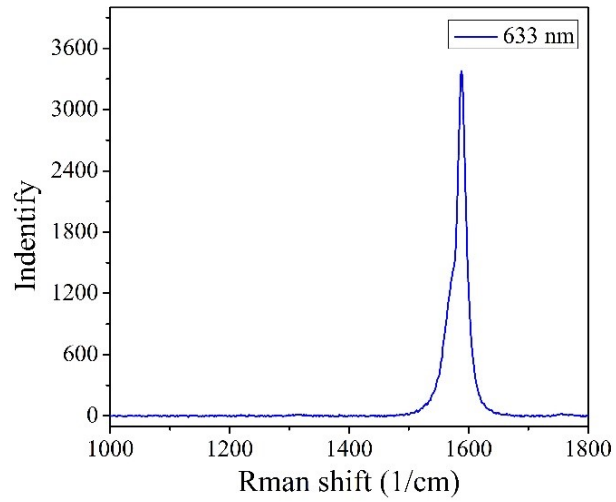


**Fig. S6.** Raman spectrum of the SB-SWCNT film with a transmittance of 85% excited with a 633 nm laser.

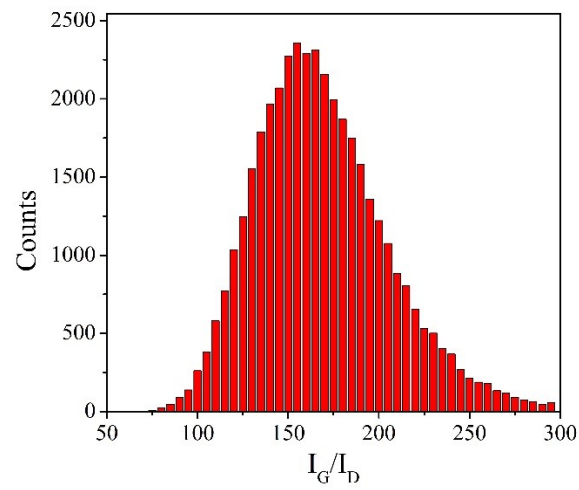


**Fig. S7.** Distribution of  $I_G/I_D$  values of the SB-SWCNT film with a transmittance of 85%.



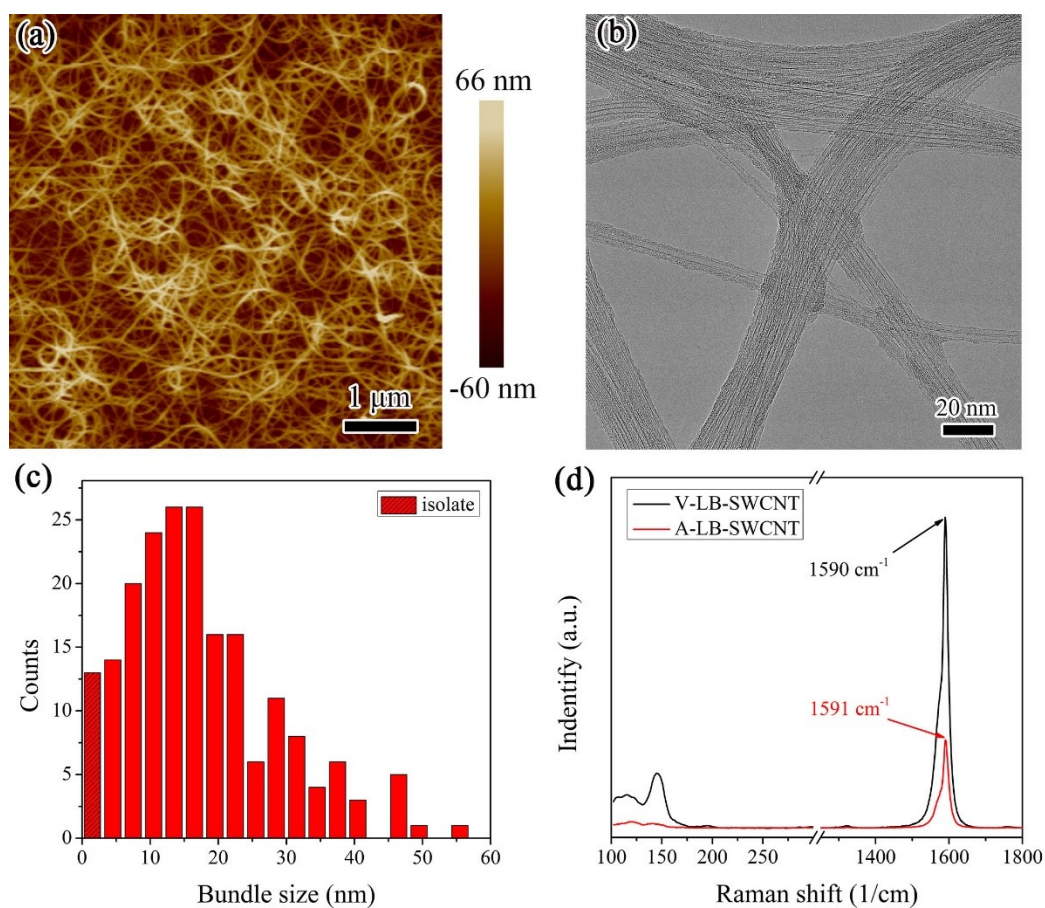


**Fig. S8.** Typical (a) AFM image, (b) TEM image, (c) bundle size distribution and (d) Raman spectra (excited with a 633 nm laser) of the LB-SWCNT film.

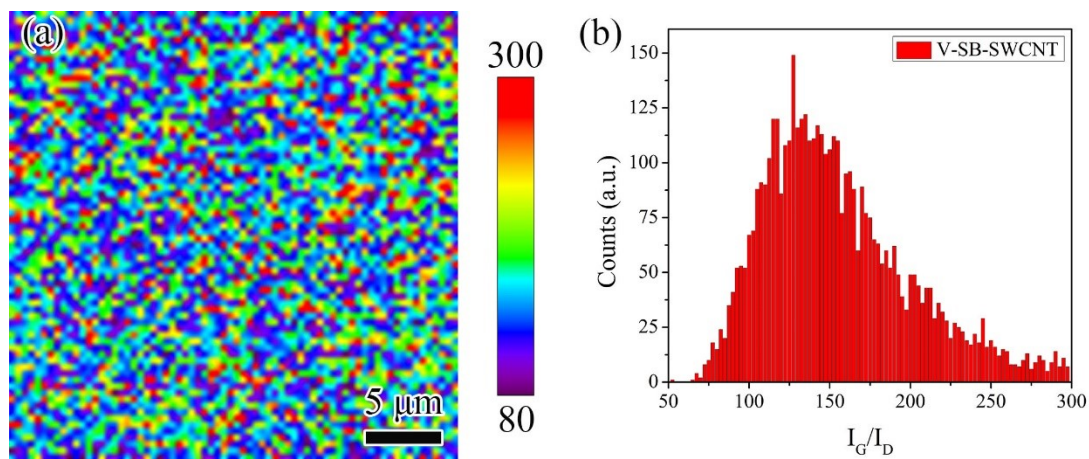


**Fig. S9.** (a)  $I_G/I_D$  mapping of V-SB-SWCNT film measured in a  $30 \times 30 \mu\text{m}^2$  area with a step of 430 nm. (b) Distribution of  $I_G/I_D$  values of the V-SB-SWCNT film with a transmittance of 85%.

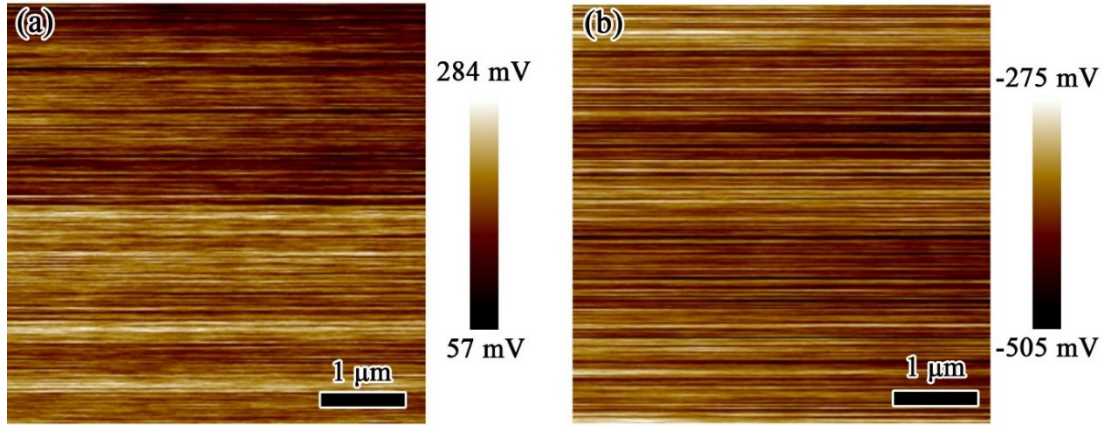


**Fig. S10.** Surface potentials of (a) A-SB-SWCNT and (b) V-SB-SWCNT Films.

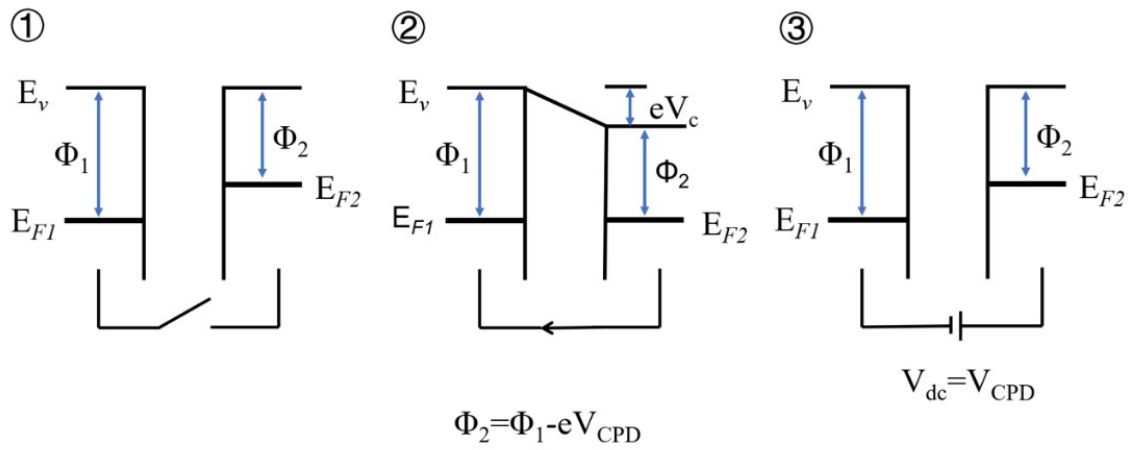


**Fig. S11.** A schematic showing the Kelvin method for the calculation of work function.

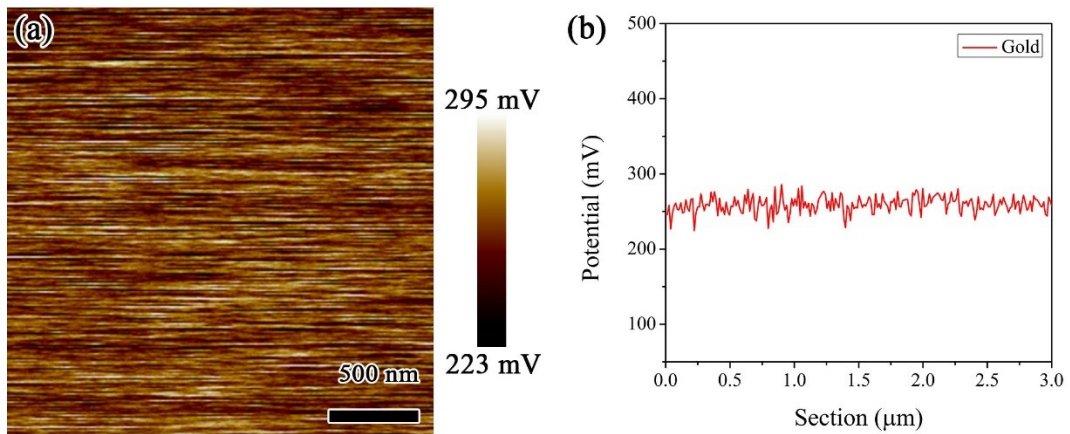


**Fig. S12.** (a) Surface potential distribution and (b) potential profile of gold film.

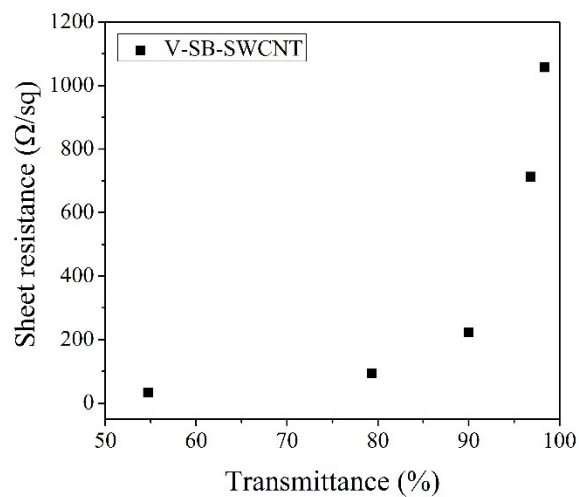


**Fig. S13.** Dependence of square resistance on the transmittance of the V-SB-SWCNT films.

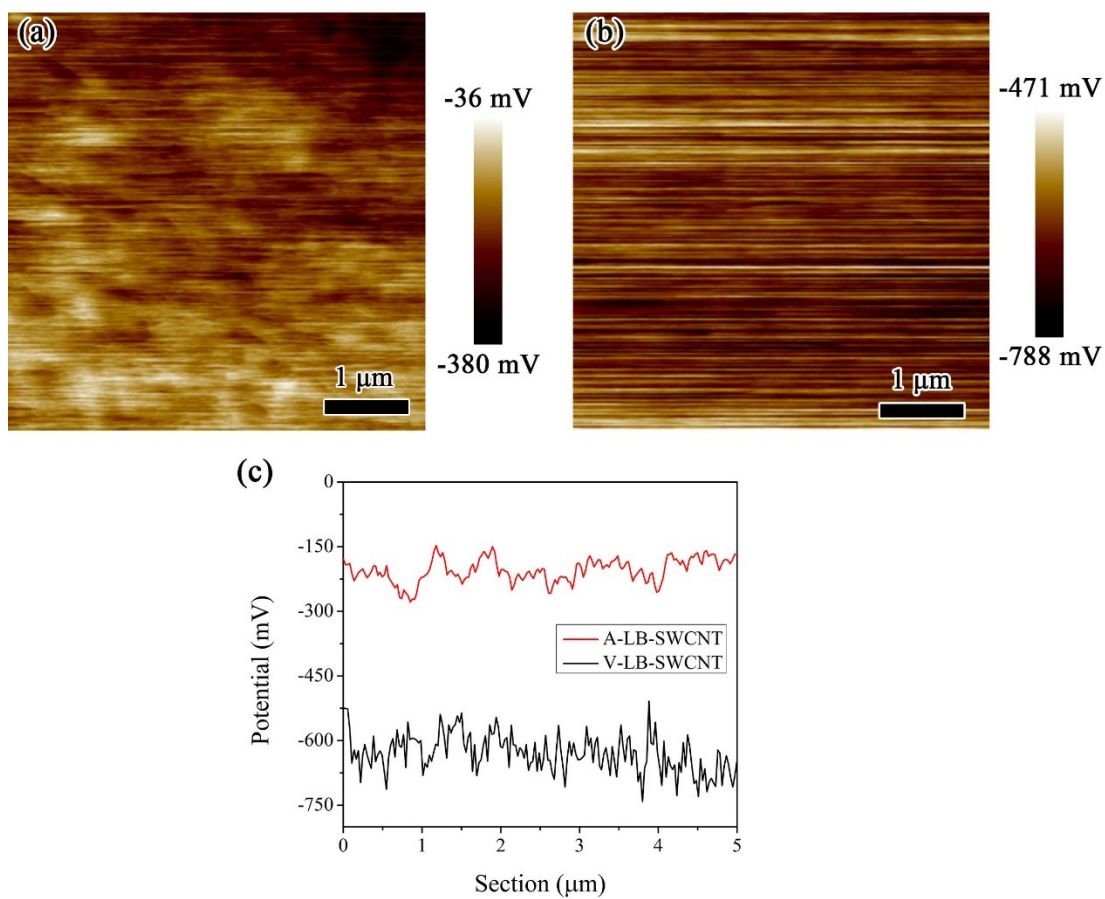


**Fig. S14.** (a) Surface potential distribution of A-LB-SWCNT film. (b) Surface potential distribution of V-LB-SWCNT film. (c) Potential profiles of A-LB-SWCNT and V-LB-SWCNT films.

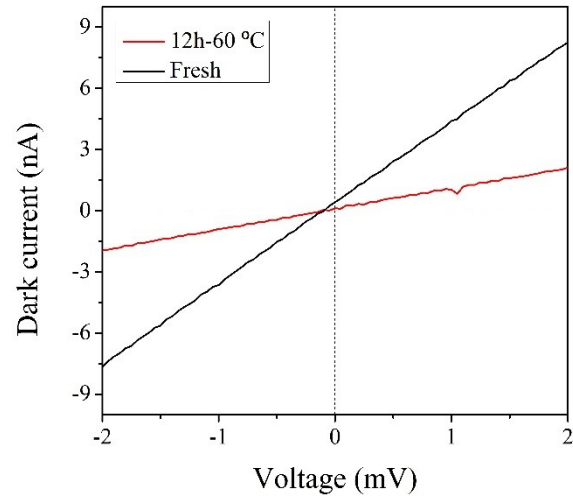


**Fig. S15.** Effect of oxidation treatment on the dark current of the SB-SWCNT-based photodetector.

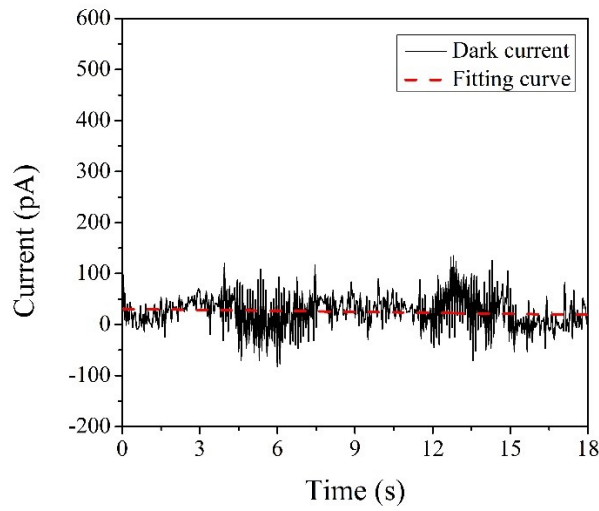


**Fig. S16.** The dark current of a photodetector fabricated using an A-SB-SWCNT film with 85% transmittance at 0 bias voltage.

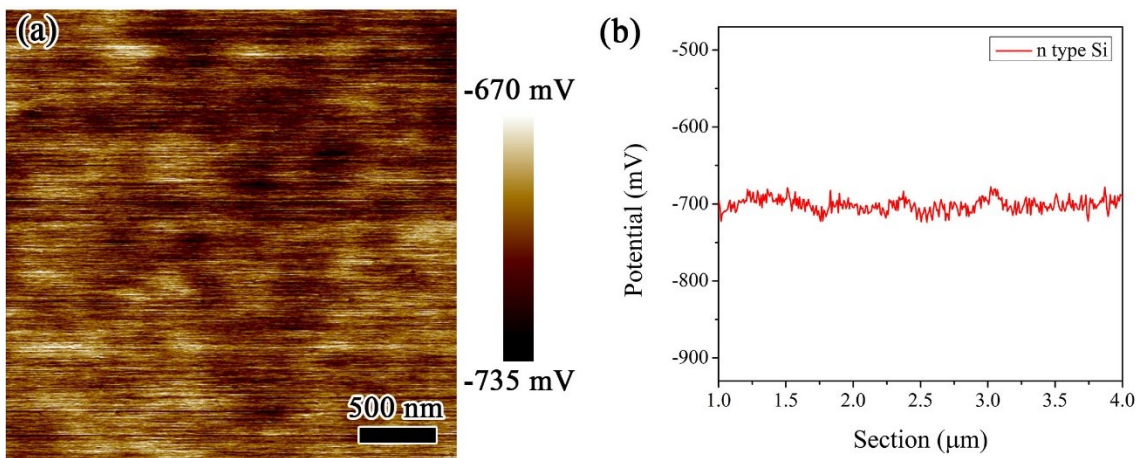


**Fig. S17.** (a) Surface potential distribution and (b) potential profile of Si.

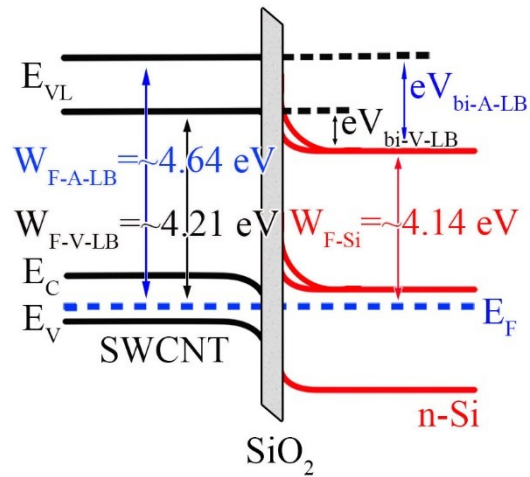


**Fig. S18.** Energy band diagram of the A(V)-LB-SWCNT/Si photodetectors.

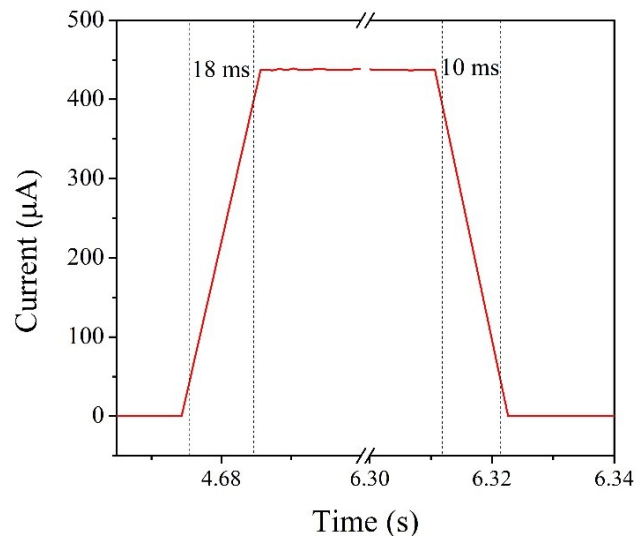


**Fig. S19.** Response and recovery times of the A-SB-SWCNT/Si heterojunction photodetectors.

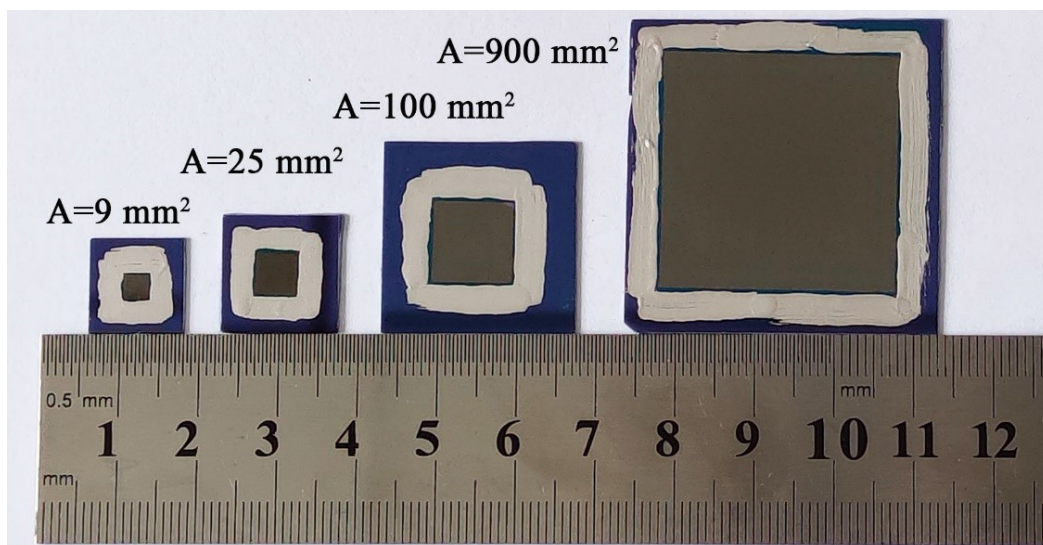


**Fig. S20.** Optical images of A-SB-SWCNT/Si heterojunction photodetectors with different window areas.

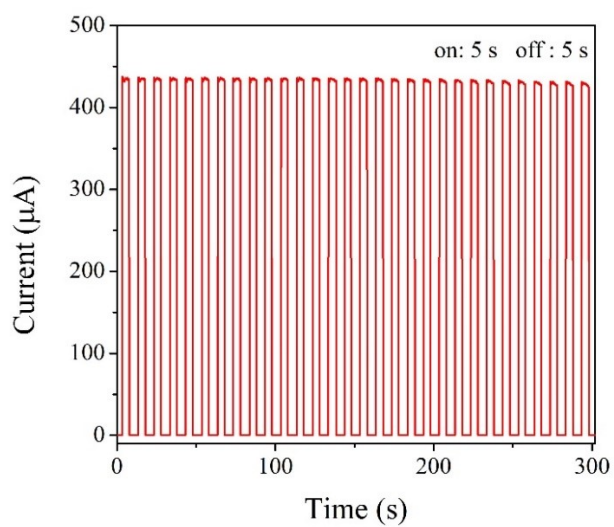


**Fig. S21.** Cyclic photo response of the A-SB-SWCNT/Si heterojunction photodetector.

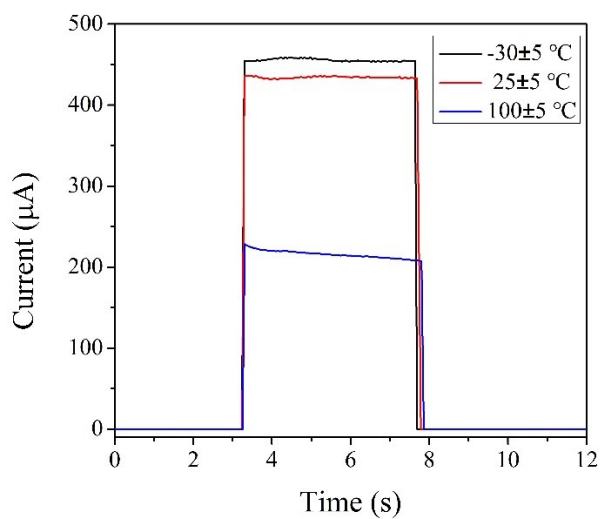


**Fig. S22.** Photo response curves of the A-SB-SWCNT/Si heterojunction photodetectors at different temperatures.